Available online at www.sciencedirect.com
ScienceDirect
Trans. Nonferrous Met. Soc. China 29(2019) 2128−2140
Transactions of Nonferrous Metals Society of China
www.tnmsc.cn

Effect of jet milling on micro-strain behavior and rupture behavior of agglomerates of ultrafine WC powders

Ya-li SUN[1,2], Qing-cai LIU[1], Xin HUANG[1,3], Fa-xing ZHANG[3], Jian YANG[1], Hua MEI[4]

1. College of Materials Science and Engineering, Chongqing University, Chongqing 400044, China;
2. College of Materials Science and Engineering, Sichuan University of Science and Engineering, Zigong 643000, China;
3. College of Chemical Engineering, Sichuan University of Science and Engineering, Zigong 643000, China;
4. Zhuzhou Cemented Carbide Cutting Tools Co., Ltd., Zhuzhou 412007, China

Received 5 January 2019; accepted 5 May 2019

Abstract: The Williamson−Hall and uniaxial compression methods were used to study the variations of the micro-strain and stress−strain relations in WC powders after jet milling and ball milling, respectively. The rupture behavior of agglomerates in WC powders was investigated. Meanwhile, the as-obtained WC powders treated by different milling methods were used to fabricate WC−10%Co cemented carbides, followed by the performance assessment of cemented carbides. The results show that the micro-strain of the jet-milled WC powders decreases significantly compared with that of the ball-milled WC powders, and that the cemented carbides prepared by jet-milled WC powders exhibit excellent properties with a transverse-rupture strength of 4260 MPa, due to the elimination of agglomerates and the reduction of lattice strain.

Key words: ultrafine WC powder; micro-strain; stress−strain relation; jet milling; agglomerate rupture mechanism

1 Introduction

Comminution is a crucial unit operation in the refractory metals industry, but a fundamental understanding of all the phenomena involved is still lacking, especially in the case of ultrafine WC powders [1,2]. In recent decades, the crucial effects of the physical characteristics of various tungsten oxides used to produce ultrafine WC powders have been investigated to improve, refine and homogenize ultrafine WC powders. And, violet tungsten oxide (TVO, $WO_{2.72}$) has been reported to be a good precursor in the production of ultrafine and homogeneous WC powders, because of its special particle morphological structure, i.e. the wedge-shaped, pore structure of the powder particles, which allow easier access for H_2O and H_2 into the pores [3].

However, the decomposition of the $WO_{2.72}$ powder usually results in whiskers with two morphologies, randomly oriented whiskers and clusters of whiskers, which produce WO_2 agglomerates [4]. These WO_2 agglomerates usually contain several small primary crystals, which are interlinked by chains of larger primary crystals [4,5]. Unfortunately, it has been reported that the reduction of the agglomerated WO_2 to tungsten is achieved without any further morphological change, so that these agglomerates are retained during the final carburization of tungsten to tungsten carbide [4,6]. In addition, these agglomerates can be retained as coarse heterogeneities in ultrafine powder matrix during further processing, which can lead to microstructural defects in the final products because of the reduction of surface energy [7].

Traditionally, ball milling is a common method to reduce the particle size and eliminate particle agglomerates of powders [8]. However, ball milling always produces a limited particle size, beyond which no further comminution occurs [9]. Furthermore, WC powder particles will undergo severe plastic deformation when the powder particles are trapped between colliding balls during the ball milling process. In consequence, it

Foundation item: Project (2016GZ0290) supported by the Key Technology R&D Program of Sichuan Province, China; Project (2019CDXYCL0031) supported by the Fundamental Research Funds for the Central Universities, China
Corresponding author: Xin HUANG, Tel: +86-13608158070, E-mail: hxwilliam@126.com;
Qing-cai LIU, Tel: +86-13608384583, E-mail: liuqc@cqu.edu.cn
DOI: 10.1016/S1003-6326(19)65119-8

causes material flaws, including a high density of lattice defects, and in particular, lattice dislocations [10]. Other significant disadvantages associated with the ball milling operation include difficulty in reproducing a particle size distribution and irregularities in shape resulted from the increase of milling time [11,12]. In addition, particle agglomeration has been evident during ball milling [8,13−15].

Recently, LI et al [16] suggested that the properties of tungsten powders could be effectively improved by jet milling treatment. In fact, jet milling has the ability to produce particles in tight size distribution, and is eco-friendly [17]. LECOQ et al [18] have studied the fracture behavior of three types of materials produced by jet milling and concluded that jet milling was suitable for processing brittle materials. Furthermore, SHAIBANI and GHAMBARI [19] have found that jet milling is much more efficient than ball milling when it is used to process brittle grey cast iron scrap into powder. The complexity, size reduction process, particle properties and the interaction between the WC powders and the jet milling process are worthy of an in-depth investigation for the lack of related reports in the literature currently. In general, smaller particles are more difficult to break than larger ones, since smaller particles contain fewer flaws and require more impact events to affect their fracture [20,21]. By contrast, larger particles commonly have many flaws, faults and discontinuities that are depleted during the formation of daughter fragments [21]. Usually, jet milling is usually not suitable for producing ultrafine grade particles since it is suitable for producing large size particles in a range of 1−10 μm [22]. However, recently LI et al [16] have found out that the big agglomerates in fine tungsten powders are absent after a jet milling treatment, which is consistent with the reported results in Ref. [23]. As is well known, the agglomeration of particles is a major problem when dealing with particles that are less than 1 μm. These agglomerates can compromise the properties of the final products. Consequently, it is important to investigate effect of jet milling on the comminuting of agglomerates in ultrafine grade WC powders. Therefore, in this work, the effects of jet milling on the comminuting of agglomerates in ultrafine grade WC powders were studied and the effects of the grinding parameters on the properties of the resulting powders were explored.

2 Experimental

2.1 Sample preparation

The ultrafine WC powders used in this work are supplied by Zigong Cemented Carbide Corp., Ltd. The powders are ultrafine grade with a manufacturer reported particle size of 0.6 μm. The powders are derived from hydrogen reduced $WO_{2.72}$ that is obtained from calcined APT (ammonium para-tungstate). Pure Co powder with a reported particle size of 0.5 μm is provided by Create Corp., China. The ultrafine WC powders (0.6 μm) are pretreated by both ball milling (milling time: 12, 24, 36, 48, 60 h, respectively; the mass ratio of milling media to powder: 10:1; rotation speed: 200 r/min) and fluidized bed jet milling. Ball-milled powders are designated as WCB, while the jet milling powders are marked as WCJ.

To compare the properties of the experimental WC powders (untreated WC, WCB and WCJ), three types of WC−Co−VC−Cr_3C_2 cemented carbide samples are fabricated through using the mentioned WC powders as raw materials, respectively. In all cases, the Co content (mass fraction) of the cemented carbides is 10%, and all the samples contain 0.4% V and 0.4% Cr (mass fraction), which originate from VC and Cr_3C_2, respectively. After milling, the powder mixtures are granulated and pressed into compacts at 200 MPa, followed by sintering from 1370 to 1410 °C using sintering−HIP (hot isostatic pressing) technology with the first stage at total pressure <5 Pa and the second stage at a total pressure about 5 MPa.

2.2 Experimental procedures

The jet milling process is performed in air using a QYF−260 fluidized bed jet mill with a dynamic classifier installed at the top of the crushing chamber of the jet mill. The process flow for the QYF−260 fluidized bed jet mill is shown in Fig. 1. The jet mill is mainly composed of an air compressor, a gas tank, a freeze dryer, an airflow crusher chamber, a cyclone separator, a pulse collector,

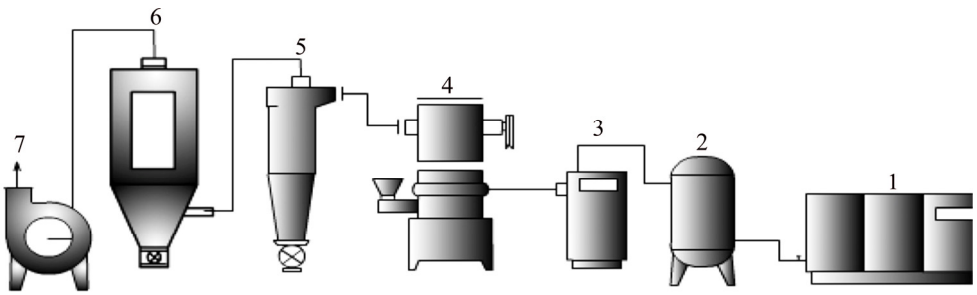

Fig. 1 Flow diagram for fluidized bed jet mill system: 1—Air compressor; 2—Gas tank; 3—Freeze dryer; 4—Airflow crusher chamber; 5—Cyclone separator; 6—Pulse collector; 7—High pressure induced draft fan

and a high pressure induced draft fan and other components.

Ball milling of the WC−Co mixtures is conducted using 1 L cylindrical cemented carbide ball mill (wet grinding media: absolute ethyl alcohol; ball: WC−8%Co cemented carbide ball). All the sets of the WC−10%Co cemented carbides are mixed with 1.5% paraffin and then pressed at 200 MPa in dies and sintered in vacuum furnace according to the traditional ultrafine cemented carbide manufacturing process.

2.3 Sample characterization

The milled and un-milled WC powders are analyzed by X-ray diffractometry (XRD) employing a D2 PHASER diffractometer (Bruker AXE, Germany). Subsequently, the resulting data are used to determine the crystallite size and lattice strain of the powders using the Williamson−Hall method. In addition, compression tests of the WCJ powders, WCB powders and un-milled WC powders are conducted using an 809 axial/torsional test system (MTS Systems Corporation, America). The morphologies and microstructures of the powders are examined using a VEGA3SBU scanning electron microscope (SEM). The Fisher particle average size (F_{sss}) is measured using a WLP−202 particle analyzer, and the particle sizes are also determined using an LMS−30 laser particle analyzer. The powder particle size distribution is determined using the gravitational sedimentation method employing a B-type turbidimeter. The specific surface areas of the particles are determined by the nitrogen gas adsorption method using an F-Sorb 2400 BET analyzer.

The coercive intensities of sintered WC−10%Co cemented carbides are measured using a YSK−IV coercive force tester. The average sizes of the WC grains in the cemented carbides are obtained using the point counting method from the micrographs. The hardness of the carbides is measured using an HR−150B Rockwell hardness tester, and transverse-rupture strength (TRS) is determined using a WB−100 universal testing machine.

3 Results and discussion

3.1 Particle morphology

The morphologies of the $WO_{2.72}$ powders are shown in Fig. 2(a) (low magnification) and Fig. 2(b) (high magnification), which depict randomly oriented, short columnar morphologies and bundles with a specific orientation. The formation of bundles or short columnar morphologies of the $WO_{2.72}$ has been attributed to the chemical vapor transport of tungsten atoms via the $WO_2(OH)_2$ vapor phase and vapor−solid reaction [3,24]. Figure 2(c) shows the morphology of the W powders that are hydrogen-reduced from $WO_{2.72}$, and the granulated shape of the W powders is clearly visible. The bundle or column of $WO_{2.72}$ is a high-aspect-ratio phase and represents an unstable morphology. Therefore, it has a spontaneous thermodynamic tendency to disintegrate into particles during the phase reduction of $WO_{2.72}$ to W powder (Fig. 2(c)) [3,25]. The morphologies of various WC powders are shown in Fig. 2(d) (low magnification) and Fig. 2(e) (high magnification). Some of the typical morphological peculiarities of the ultrafine W and WC powders are their pseudo-morphology appearance relative to the starting oxides, which indicates that a physical contact exists between the metal and carbide particles. This physical contact will produce agglomerates of W or WC, attributed to chains of primary crystals [4,5], as shown in Fig. 2(e) and Fig. 2(d). In addition, the size distribution curve (Fig. 2(f)) of the ultrafine WC particles is remarkably broadened with a long “tail”, indicating the existence of a few large size WC particles in the ultrafine WC powders.

The properties of the WC, W and $WO_{2.72}$ powders are provided in Table 1. As shown, they all present good consistency between the LMS particle size and Fisher particle size. It should be noted that the laser particle analyzer has a lower limit of measurement in measuring the particle size distribution, whereas the sedimentation method has no theoretical minimum dimension measurement [26]. Therefore, the finest particles in the ultrafine WC powders cannot be measured using the laser particle size analyzer. Furthermore, if the proportion of this kind of powders is larger in the ultrafine WC, the measurement error using laser particle size analyzer will be greater. In this work, the particle size distribution of the ultrafine WC powders is determined using the sedimentation method. And, BET particle size can be calculated according to S_{BET} data in Table 1 and the calculated BET particle size of WC powders is 0.13 μm, from which it can be seen that the agglomeration of the WC powders is serious since the LMS particle size and F_{sss} of WC powder are 0.52 and 0.71 μm, respectively.

3.2 Jet milling of ultrafine WC powder

A circular gas flow is adopted to break up the large powder agglomerates via particle−particle collision, particle−wall collision, and the shear force in the high-velocity jet stream in fluidized bed jet mill system [27]. In general, jet milling is not suitable for pulverizing smaller particles, because smaller particles contain fewer flaws and require more events to break them down [20,21]. But, recently LI et al [16] found that a fluidized bed jet mill is effective for pulverizing agglomerates in smaller particles. Based on their research, the illustration of the concept behind the fracture of ultrafine WC agglomerates at high grinding gas pressure is shown in Fig. 3. At high grinding gas

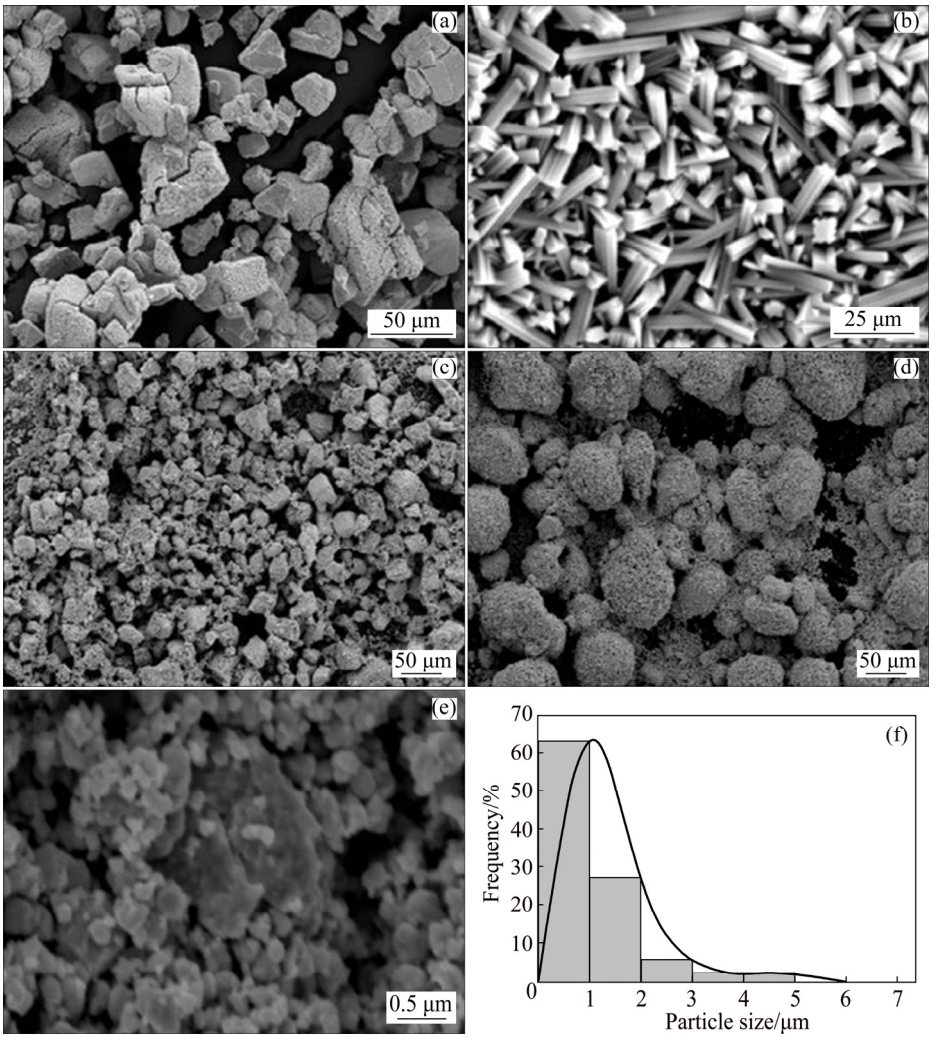

Fig. 2 SEM images from $WO_{2.72}$ to W powders: (a) $WO_{2.72}$ powders (low magnification); (b) $WO_{2.72}$ powders (high magnification); (c) W powders; (d) WC powders (low magnification); (e) WC powders (high magnification); (f) Particle size distribution of WC particles

Table 1 Properties of WC, W and $WO_{2.72}$ powders

Sample	F_{sss}/μm	S_{BET}/($m^2 \cdot g^{-1}$)	LMS particle size/μm	w(O)/%
$WO_{2.72}$	12.82	1.30	–	–
W	0.92	3.55	0.85	0.38
WC	0.71	2.79	0.52	0.33

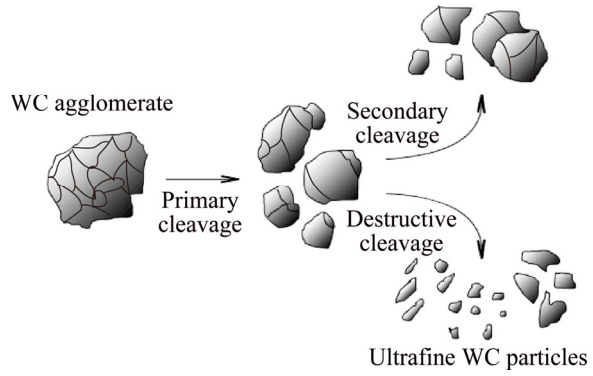

Fig. 3 Illustration of agglomerate breakage process

pressure, the agglomerates are accelerated to high velocity. The fracture of these large agglomerates will be caused by their impact and cleavage into blocks during the following steps: primary cleavage, followed by secondary cleavage and destructive breakage (Fig. 3). At a lower grinding gas pressure, the agglomerate acceleration is lower, and the particles rub each other, causing the trimming of the edges of large agglomerates [20,22,28,29].

3.2.1 Grinding gas pressure

Figure 4 shows the SEM images of the ultrafine WC powders as a function of various grinding gas pressures, i.e. 0.2, 0.4, 0.6, and 0.8 MPa, illustrating the evident effect of gas pressure on the cleavage of the agglomerates. Figure 2(d) shows the morphology of the original ultrafine WC powders containing large, pseudo-crystals (agglomerates). Grinding the WC powder at lower gas pressure will usually increase the likelihood of abrasion between agglomerates and powders [20,22,28,29]. At the

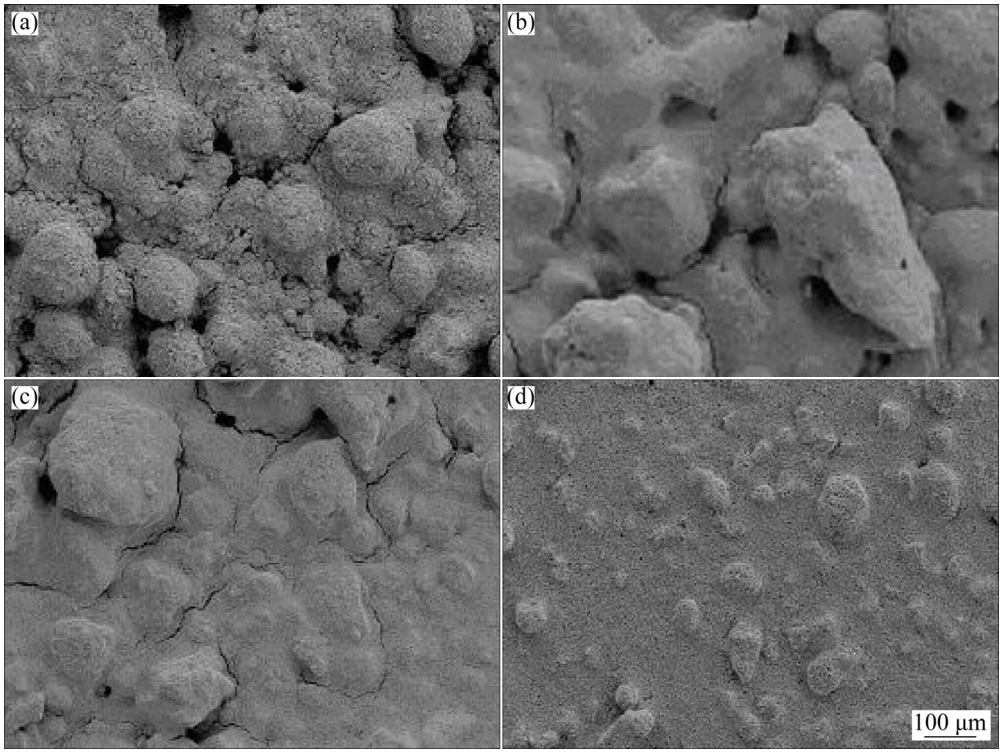

Fig. 4 SEM images of jet-milled WC powders under different grinding gas pressures: (a) 0.2 MPa; (b) 0.4 MPa; (c) 0.6 MPa; (d) 0.8 MPa

lower grinding gas pressures of 0.2 and 0.4 MPa, it can be seen from the images in Figs. 4(a) and (b) that some of the smaller agglomerates begin to be fractured and converted into powders. As the grinding gas pressure is increased from 0.6 to 0.8 MPa, most of the agglomerates disappear, and the particles are more dispersive (Figs. 4(c) and (d)). At the higher grinding gas pressure, the agglomerates and powders are accelerated to high velocity, which enhances the particle collision and breakage, resulting in a huge decrease in the number of agglomerates. However, in industrial practice, as the grinding pressure increases, the energy input to the process will significantly increase. For example, only 1 kW·h/t is required to produce particles of 10^4 μm size, while more than 200 kW·h/t is required to obtain 1 μm size particles [21]. In this work, a grinding gas pressure of 0.8 MPa is used to balance good pulverization with energy efficiency.

3.2.2 Rotation speed

In jet milling process, the powder particles are simultaneously subjected to the airflow drag force and rotating centrifugal force in the classifier chamber [27]. When the centrifugal force is greater than the drag force, the coarser particles will not enter the inner classifier chamber, but instead, return to the grading chamber. On the other hand, when the centrifugal force is smaller than the drag force, the finer particles can be transported by the airflow through the rotor and collected by the collector. The so-called cut size is particle or agglomerate size for which the centrifugal force is equal to the drag force, and the value of cut size d_c can be simply estimated by Eq. (1) [30,31]:

$$d_c = \frac{k}{n}\sqrt{\frac{Q}{\rho_s}} \tag{1}$$

where ρ_s is the density of WC powders; Q is the gas flow rate through the classifier; k is the coefficient taking consideration of air viscosity and constant of blade shape; n is the classifier/rotor rotating speed. It can be concluded from Eq. (1) that the cut size d_c is inversely proportional to the classifier rotating speed, and the rotating speed should increase as the particle or agglomerate size decreases.

Figure 5 shows the powder morphology and particle size distribution of the milled product at different rotation speeds. At rotation speeds of 2000 and 4000 r/min, some agglomerates are present in the product as shown in Figs. 5(a_1, b_1). In addition, the particle size distribution curves are broadened with large particle size in the range of 4−5 μm (Figs. 5(a_2, b_2)). When the rotation speed reaches 6000 r/min and above, fewer agglomerates are observed in the products, in which the large particle size reduces to 1−2 μm (Figs. 5(c_1, d_1)). Moreover, the particle size distribution curves become tighter as the rotating speed increases, and the "long tail" in the particle size distribution curves disappears

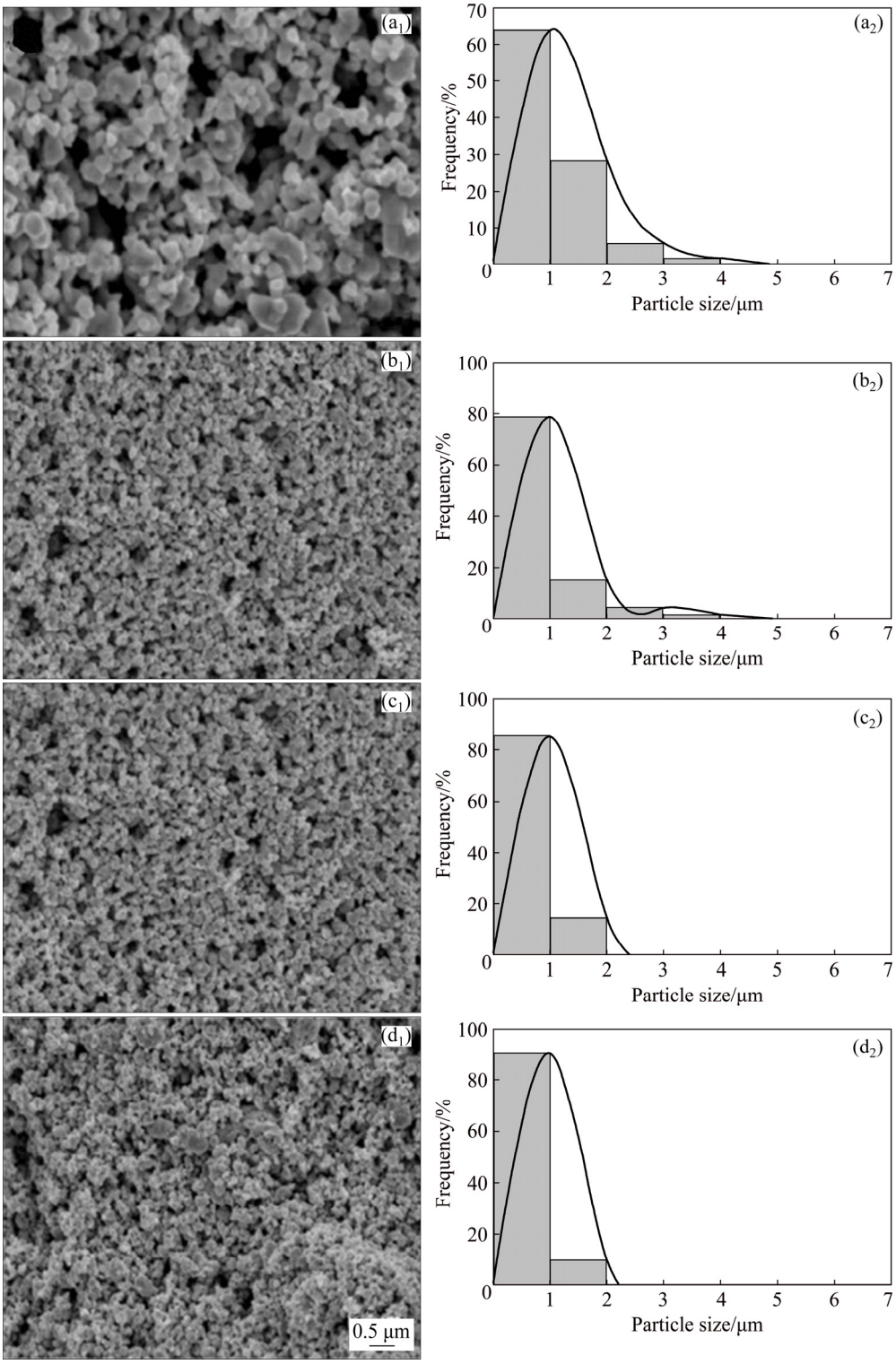

Fig. 5 SEM images (a_1−d_1) and particle size distribution (a_2−d_2) of jet-milled WC powders at different rotation speeds: (a_1, a_2) 2000 r/min; (b_1, b_2) 4000 r/min; (c_1, c_2) 6000 r/min; (d_1, d_2) 8000 r/min

(Figs. 5(c_2, d_2)). The tighter particle size distribution curves indicate that most of the large particles and agglomerates are fractured, resulting in an increase in the number of small particles. Therefore, it can be concluded that a higher classifier rotation speed will produce a smaller average particle size and a tighter particle size distribution, which is in good agreement with Eq. (1) as derived from the theory of centrifugal grading.

3.2.3 Jet milling times

The ultrafine WC powders are ground three successive times at a grinding gas pressure of 0.8 MPa and a rotation speed of 8000 r/min in the jet mill.

Figure 6 shows the effect of jet milling repetition on the Fisher particle size and specific surface area of the ultrafine WC powder product. Clearly, the Fisher particle size of the WC powder is significantly reduced after the first jet milling, but the Fisher particle size of the WC powder does not significantly change in the successive second and third jet milling. This is probably because the agglomerates in the powders are significantly comminuted in the first jet milling. So, the successive jet milling has little effect on the particle size of WC powder. However, ultrafine WC powder is likely fractured by abrasion after the comminuting of agglomerates in the powders. WANG and PENG [28] investigated the comminuting behavior of fine powders and reported that fine particles with fewer flaws, cracks, crystal boundaries and higher specific surface energy possess higher mechanical strength and are more structurally stable. Thus, fine particles cannot be thoroughly fractured to even finer pieces. On the other hand, WC exhibits abrasion resistance because it is a very hard material with very strong covalent bonding. Therefore, it is illustrated that abrasion in the first jet milling is the main mechanism of the particle fracturing since the WC powders are observed to have almost no change in the Fisher particle size after the second and the third jet milling. In addition, the specific surface area results of the WC powders are shown in Fig. 6, which show a slight increase with successive jet millings. This probably results from the additional abrasion that produces additional new particle surfaces.

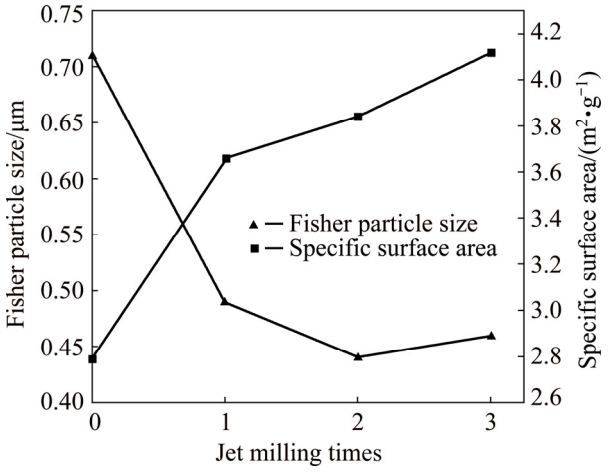

Fig. 6 Relationship between Fisher particle size/specific surface area and jet milling times

3.3 Comparison of jet milling and ball milling

It has been reported that ball milling operation has worked well for breaking up of large particles, but not for fracturing sub-micrometer particles [32]. And, fracturing is the major mechanism during ball milling, which always leads to high distortion of WC particles [6]. Since the research on the WC ball milling is quite extensive, the main purpose of this work is to compare the properties of ball-milled powders with those of the jet-milled powders, to provide a better understanding of the jet milling process. For ball milling of the WC powder, based on previous experience, typical milling time of 24, 36, 48 and 60 h is selected with a rotation speed of 200 r/min and a ball-to-powder mass ratio of 10:1. X-ray diffraction patterns of the ball-milled WC powders prepared with different milling time are presented in Fig. 7. As shown, the sharpness of the peaks clearly increases with the increase in milling time, which is due to the increase in the milling energy. Figure 7 also shows that the W_2C phase in the original powder disappears when the ball milling time reaches 48 h. Since finer particles usually possess higher surface energy, they are more reactive with carbon in the environment; consequently, as the milling energy increases, the fine powder particles react with the carbon in the cemented carbide milling balls.

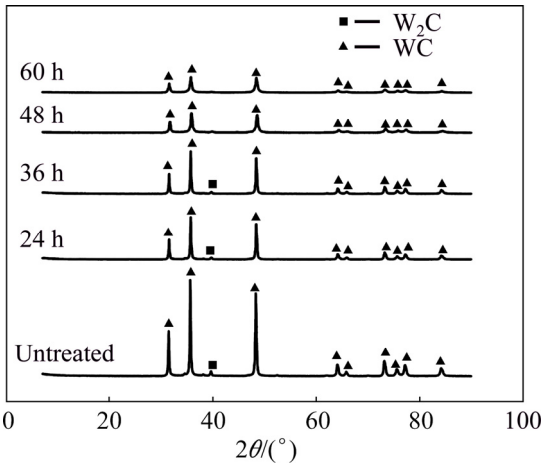

Fig. 7 XRD patterns of different WC powders

3.3.1 Average crystallite size and strain of WC powders

Figure 8 displays the results of the Williamson−Hall analysis of the XRD data [33]. As can be seen from these results, the increase in the number of jet milling processes produces a slight decrease in crystallite size, whereas the strain is steady. Also, the data in Fig. 8 show that the untreated WC powders obtained from the $WO_{2.72}$ have a lattice strain about 0.15% and a crystallite size of 56 nm. After jet milling, the lattice strain of this powder decreases to 0.1%, while the crystallite size is stable in the range of 60−65 nm. So, the lattice strain of the powder decreases while crystallite size does not change obviously after jet milling. By contrast, PALANIANDY et al [20] have reported that jet milling produced a smaller crystallite size and higher lattice strain of this fine powder. However, no substantial changes in the crystallite size of the ultrafine WC powder are observed in our experiment, and the lattice strain is significantly

reduced after the jet milling. This suggests that jet milling has exclusive effect on ultrafine and fine powders. The decrease in the lattice strain of the ultrafine WC powder is partially the result of the release of accumulated stress caused by the comminuting of the agglomerates. But, this drop in strain does not increase with additional jet milling time. There is no significant decrease in the lattice strain of the WC powder after the first jet milling. Figure 8 also shows that the crystallite size of the WC powder continues to decrease with the increase in ball milling time, while the lattice strain continuously increases. During the ball milling process, the powders are subjected to high energy collision, which produces plastic deformation and fracture. The crystallite size decreases as a result of the formation of correlated arrangements of the defects, such as dislocation walls or small-angle grain boundaries (sub-grain), which also causes an increase in the lattice strain. The presence of high density of microstructure defects in WC powder is evident from the line broadening of WC X-ray peaks, which can be clearly seen in Fig. 7.

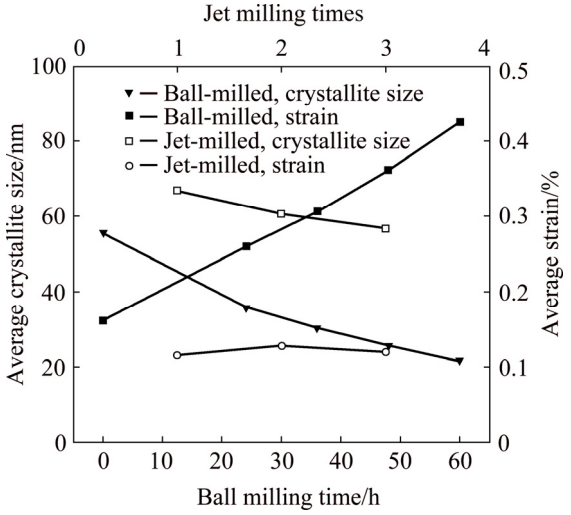

Fig. 8 Relationship between average crystallite size/strain of WC powder and ball milling time/jet milling time

Figure 8 also shows that the crystallite size decreases quickly from 56 to 30 nm after the ball milling time increases from 0 to 36 h, and the decrease in the crystallite size begins to slow down from 30 to 22 nm when the ball milling time increases from 36 to 60 h. This indicates that the formation of sub-grains becomes more difficult during the continuous ball milling. Since the research on the WC ball milling is quite extensive, the main purpose of this work is to understand the characteristics of the jet milling process. Therefore, a good way to understand the effect of jet milling process on the properties of WC powder is to compare the results with those data obtained from the well-studied ball milling process. The ball milling is conducted for 36 h at a rotation speed of 200 r/min, while one jet milling is conducted at a grinding gas pressure of 0.8 MPa and a rotation speed of 8000 r/min.

3.3.2 Particle size distribution and morphology

After ball milling, a significant quantity of WC agglomerates are clearly visible in Fig. 9(a), which is consistent with the observations of BROOKES [9] and GUO et al [34]. These authors conclude that for a given set of milling conditions an “equilibrium” might occur where further comminution of the powder is balanced by its agglomeration. Also, the ball milling produced a limited grain size, beyond which no further comminution would occur [9]. However, it is found in this work that most of the agglomerates disappear after jet milling, as shown in Fig. 9(b). From the SEM observations, it is also found that the WC powder is more uniform in size after jet milling, as shown in Fig. 9(d), while the WC powder pretreated using the ball milling process exhibits the existence of many agglomerates (Fig. 9(c)).

As shown in Fig. 9(e), the particle size distribution curves for the untreated WC and ball milled WC (WCB) are broadened with a “long tail”, indicating that some large aggregated particles are still present in the powder after ball milling. In addition, a tight particle size distribution curve is obtained for the jet milled WC (WCJ), as demonstrated in Fig. 9(e), illustrating the effectiveness of jet milling in reducing agglomeration.

3.3.3 Phase composition

The XRD patterns of the untreated WC, WCB and WCJ powders are displayed together in Fig. 9(f). The data suggest that no significant differences are present in the Bragg diffraction peaks for the untreated WC (Curve 1 in Fig. 9(f)) and WCJ (Curve 2 in Fig. 9(f)), while X-ray profiles of WCB (Curve 3 in Fig. 9(f)) are sharper than those of the untreated WC powder (Curve 1 in Fig. 9(f)). However, the slight increase in the crystallite size of the jet-milled WC powder (67 nm) compared to that of the untreated WC powder (56 nm) indicates that jet milling process eliminates some defects and flaws in the powder because the radical size changes of the sub-grains result from the re-arrangement of the defects, such as dislocation walls or small-angle grain boundaries. In the jet milling process, particle fracture behavior is governed largely by the pre-existing flaws and defects in the powder, and cracks grow from these flaws and defects during the stressing of the particles in the jet mill. These cracks propagate and begin to interact with one another, leading to crack coalescence and finally, particle fracture [35]. When particles are broken along the flaws, the particle size reduces (Table 2) and the particle flaw density also decreases, which is partly the result of the increase in the crystallite size of the jet-milled WC powder.

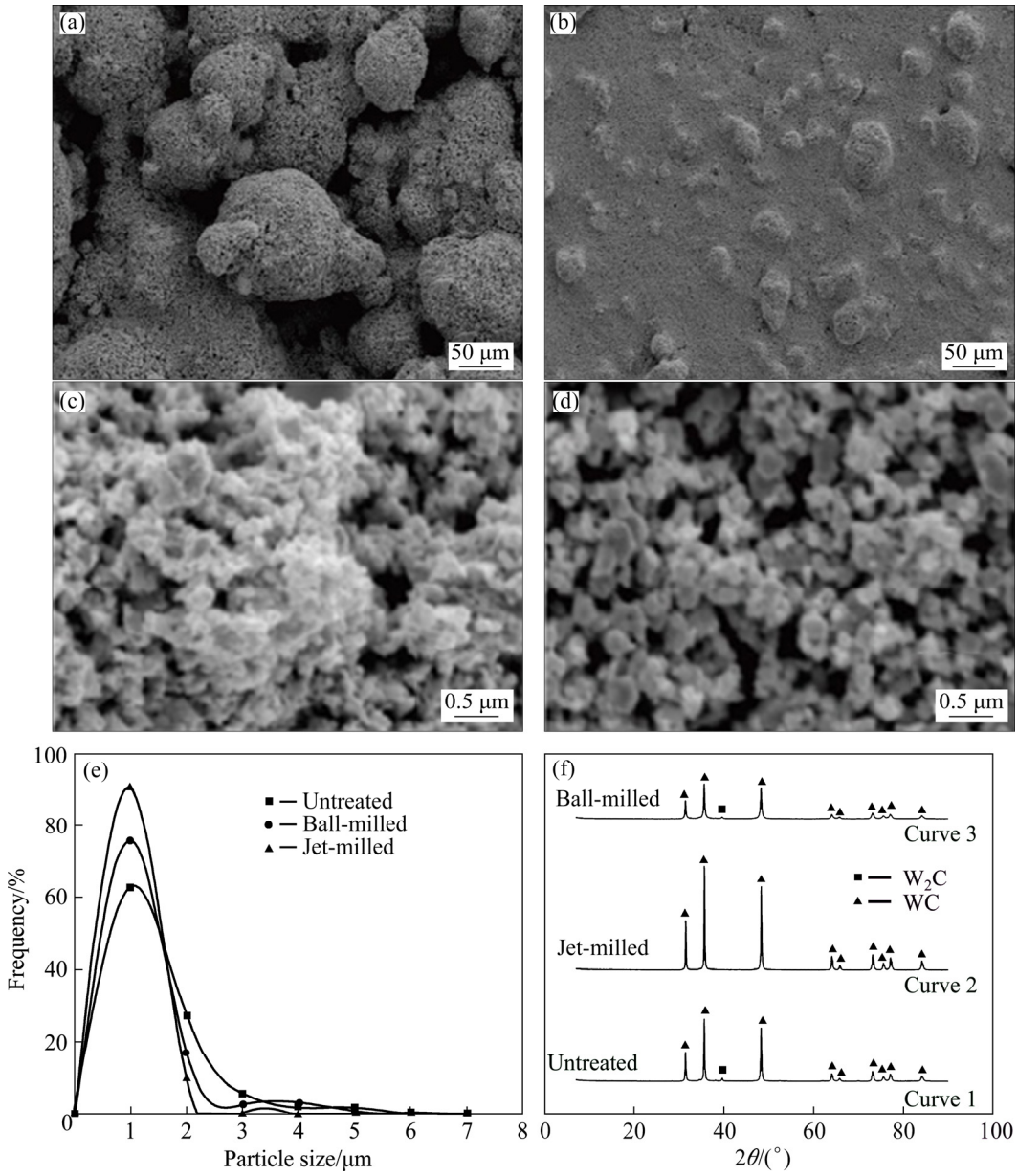

Fig. 9 SEM images, particle size distribution and XRD patterns of different WC powders: (a) WC powder pretreated by ball milling (low magnification); (b) WC powder pretreated by jet milling (low magnification); (c) WC powder pretreated by ball milling (high magnification); (d) WC powder pretreated by jet milling (high magnification); (e) Particle size distribution curves of different WC powders; (f) XRD patterns of different WC powders

Table 2 Physical properties of different powders

Sample	F_{sss}/μm	S_{BET}/($m^2 \cdot g^{-1}$)	w(O)/%
WC (Untreated)	0.71±0.13	2.79±0.38	0.33±0.02
WCB (Ball-milled)	0.58±0.18	3.18±0.46	0.42±0.03
WCJ (Jet-milled)	0.49±0.16	3.66±0.30	0.21±0.02

During the ball milling process, although the particles are also broken along their flaws, the particles are simultaneously subjected to high energy collision, which causes the formation of more particle defects and flaws, such as dislocations, small-angle grain boundaries, or twins [8]. Therefore, X-ray profile broadening (Fig. 7) and a significant decrease in crystallite size are observed for the WCB powder as shown in Fig. 8.

The weak diffraction peaks of the W_2C phase of ball-milled powder are clearly visible in Curves 1 and 2 in Fig. 9(f), illustrating that the carbon deficient phase of the W_2C cannot be easily removed by the ball milling process. However, the diffraction peak of W_2C phase disappears after jet milling treatment (Curve 2 in Fig. 9(f)). This result probably occurs, because W_2C particles do not enter the classifier and return to the grinding chamber due to their higher density.

Ball-milled powders contain a greater amount of

surface oxides than the jet-milled powders, as illustrated in Table 2. Also, the oxygen content of the WC powder decreases from 0.33% to 0.21% after jet milling, while the oxygen content of the ball-milled WC increases from 0.33% to 0.42%. This is because usually no fresh oxides are formed during the jet milling process due to the process conditions, i.e. room temperature and short time pulverization [36]. Furthermore, the existing surface oxides will be peeled off and sucked away during the jet milling process. Thus, impurities can be effectively removed by the jet milling process, and there are no new, additional impurities formed in the process.

3.4 Compression properties

The agglomerates present in the WC powder will affect the powder properties, including the important structural factors such as agglomerate shape, size, packing structure and coordination number of primary particles and their bonding mechanism [37,38]. One of the simple and convenient ways to understand the effects of agglomerates on the powder is to perform powder compression tests [36]. Figure 10(a) shows a schematic diagram of the device used for investigating the pressing characteristics of a WC powder containing agglomerates. The powder pressing is conducted using a mechanical testing machine to automatically record the pressure and the displacement of the beam during compression. To reduce the friction between the powder and the mold wall during compression, the height-to-diameter ratio of the powder is kept to be less than 1.0. When the pressure is P_i, the relative density of WC compact is calculated using Eq. (2) [38,39]:

$$\rho_i = \frac{m}{\left[\rho_{WC}\pi r^2\left(h_0 + L_0 - l_0\right) - \rho_{WC}\pi r^2\left(L_i - l_i\right)\right]} \quad (2)$$

where ρ_i is the compact density when the pressure is P_i; ρ_{WC} is the theoretical density of WC powder; m is the mass of a powder compact; r is the inner radius of steel die; h_0 is the final height of the compact; L_0 is the final displacement of the beam; L_i is the displacement of the beam when pressure is P_i; l_0 is the final displacement of the beam when pressure is P and there is no powder in die; l_i is the displacement of the beam when pressure is P_i and there is no powder in the die.

As Eq. (2) shows, the relative density of the compact ρ_i is inversely proportional to the displacement of the upper punch. Figure 10(b) shows the curves of applied stress versus the displacement of the upper punch during the compression process, which also represents the relationship between applied stress and compact density. As shown, the curves show three periods: Periods I, II and III. During Period I, the main agglomerate rearrangement occurs as the applied stress is increased. After the rearrangement, the main agglomerates are broken during Period II, while the main primary particle rearrangement starts to take place in Period III. Since the WCJ powder contains only a few agglomerates only a short time is required for its agglomerate rearrangement and rupture, as shown in Fig. 10(b). In general, Curve 3 is smooth, and the applied stress curve is almost linear with the displacement of upper punch after inflexion point o (Fig. 10(b)).

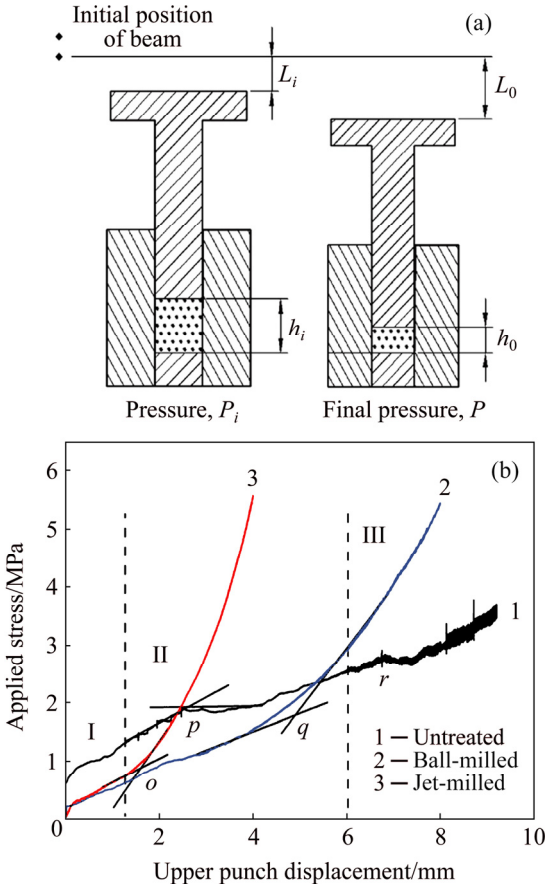

Fig. 10 Schematic diagram of device for compressing WC powders (a) and relationship between applied stress and upper punch displacement during compression of different WC powders (b)

In the case of the WCB powder (Curve 2 in Fig. 10(b)), there is a longer duration for agglomerate rearrangement and rupture than that of the WCJ, which demonstrates that the WCB powder contains more agglomerates. As shown, the applied stress curve is nearly linear in the displacement of upper punch after the inflexion point q. As illustrated by Curve 2 in Fig. 10(b), the primary particles start to rearrange in Period III after the curve has passed through point q.

The untreated WC powder contains a particularly large number of agglomerates, and the compression curve (Curve 1 in Fig. 10(b)) exhibits two inflexion points. In the initial agglomeration rearrangement period, the appearance of a fluctuation in the curve is probably

the result of the sudden rupture of agglomerates, which causes a variation in applied pressure. In Period II, many agglomerates are simultaneously fractured so that there are some jagged steps in the curve. These jagged steps demonstrate the sudden changes in applied stress, which are partly the result of continuous and rapid rupture of the agglomerates. Also, Curve 1 appears to oscillate after the inflexion point *r*, exhibiting a widening, which may be due to the initial rupture of some unbroken, hard agglomerates during Period II. The sudden rupture of hard agglomerates causes the sudden variation of pressure, which produces the sharp jump at the end of Curve 1, thereby forming a broadening zone at the end of Curve 1. These results indicate that the number of agglomerates in the powder will greatly influence the compression characteristics of the powders, and that the powders with the lowest amount of agglomerates have a flatter compression curve.

3.5 Effect of powder properties on sintering

The sintering of ultrafine WC−Co cemented carbide is a complex and still not fully understood process. However, it is clear that the characteristics of the initial WC powder have a great effect on the sintering process and the properties of the final sintered cemented carbide.

3.5.1 Strain of WC phase

There is a time when it is believed that conventional ball milling could increase the surface energy of the WC particles and this increased strain would improve the sintering ability of the powders. This theory has been discounted by experimentation, which has shown that the strain in the particles is far lower than the expected one. Consequently, it is concluded that the increased particle strain is not sufficient to constitute the driving force for sintering [9]. In addition, it has been shown that the amount of inter-lattice diffusion (mechanical alloying) between the WC phase and Co binder has a more significant effect on sintering [9]. It is not clear how the low strain of the jet-milled powder affects its sintering. However, the low strain value of the WC phase (Table 3) in the final cemented carbide clearly illustrates the benefit of jet milling to the plastic deformation of the WC phase.

3.5.2 Particle size distribution and agglomerates

Even though conventional cemented carbide sintering is based on liquid phase sintering, pronounced densification occurs even during solid-state sintering via solid state diffusion, transport of particles and the plastic flow in the carbide binder areas [40,41]. SCHUBERT et al [42] also reported that in the case of ultrafine carbides, up to 90% of the densification occurred during the solid sintering (below 1280 °C). In addition, solid-state densification will increase with decreasing particle size. Therefore, as a result of this early solid sintering mechanism, the agglomerates in the WC powders will influence the sintering characteristics of the powders.

On the other hand, in the case of Ostwald ripening, free energy change (ΔG_d) is considered to be the driving force for liquid sintering. The parameter ΔG_d is defined as the difference in the capillary pressure (or the chemical potential) between different sized WC grains [43]. Based on the Wulff theorem, KANG et al [43] proposed a simplified equation, as expressed in Eq. (3) to calculate ΔG_d.

$$\Delta G_d = 2\gamma_{sl}\left(\frac{1}{R^*}-\frac{1}{R}\right) \tag{3}$$

where ΔG_d is the driving force to coarsen the grain; γ_{sl} is the surface energy of solid/liquid for a given facet of WC grain; R^* is the critical grain size, which does not grow and dissolve at a given instant; R is the grain size defined by the distance from the center of the equilibrium shape to the given facet.

The size of the largest particles in the WC raw powders can be correlated with the driving force for coarsening as shown in Eq. (3). The various physical properties of the cemented carbides fabricated from the different WC powders are presented in Table 3. As shown, the cemented carbide made by the WCJ powders, with the smallest average grain size (0.43 μm) of the three cemented carbides, exhibits superior comprehensive properties. The main reason for this may have been the tighter particle size distribution of the jet-milled WC powders. This result agrees with the data for the WCJ powder cemented carbide that has the highest coercive force value, with the highest transverse rupture strength of 4260 MPa.

TAN and HUANG [44] proposed an equation to analyze the abnormal growth of the WC particles, which

Table 3 Properties for cemented carbides made from different powders

Sample	Density/ ($g\cdot cm^{-3}$)	Hardness (HRA)	TRS/ MPa	Coercivity/ ($kA\cdot m^{-1}$)	d_{WC}/ μm	Porosity	Strain of WC phase/%
Untreated WC	14.36±0.03	92.6±0.1	2690±196	26.5±0.6	0.51±0.22	A04B02	0.415±0.005
Ball-milled WC	14.38±0.05	92.8±0.2	3012±138	32.7±0.8	0.48±0.18	A02B02	0.620±0.005
Jet-milled WC	14.42±0.03	93.0±0.2	4260±121	36.4±0.6	0.43±0.16	A02B02	0.312±0.006

is expressed in Eq. (4):

$$\Delta F_s = \frac{2\sigma d_g}{\rho}\left(\frac{1}{R_c}-\frac{1}{r_1}\right) \quad (4)$$

where ΔF_s is the change in the value of the free energy on the surface of the solid particles, which varies with the size of WC particles; σ is the stress; ρ is the density of the WC phase; d_g is the amount of the fine WC particles produced by solution−reprecipitation; R_c is the radius of the coarse WC grains in the cemented carbide; r_1 is the radius of fine grains in the cemented carbide. Equation (4) provides a relationship between the particle size difference in the powder and the change in the free energy: the larger the ΔF_s is, the more likelihood the abnormal powder growth is. The WCJ powder has the tightest particle size distribution and contains fewer agglomerates, so that the tendency of abnormal grain growth is reduced. This more uniform grain microstructure is obtained by using jet-milled powder, and the cemented carbide made by jet-milled powder commonly displays higher comprehensive mechanical properties, such as higher strength and hardness.

4 Conclusions

(1) The results of XRD and SEM analysis indicate that the agglomerates in ultrafine WC powders obtained from the reduction of $WO_{2.72}$ can be effectively eliminated by the jet milling, and that jet-milled ultrafine WC powders have a low lattice strain of 0.1% and a tight particle size distribution.

(2) Jet-milled ultrafine WC powders exhibit a good compression behavior in the uniaxial compression test, and the compression curve is flatter and lacks any jagged step in the curve.

(3) Cemented carbide made by jet-milled WC powders exhibit higher comprehensive mechanical properties with a transverse rupture strength of 4260 MPa and an average grain size of cemented carbide is 0.43 μm. In addition, jet milling of ultrafine powders is a viable and effective technique for processing ultrafine WC powder.

References

[1] LECOQ O, CHAMAYOU A, DODDS J A, GUIGON P. Application of a simplifying model to the breakage of different materials in an air jet mill [J]. International Journal of Mineral Processing, 2012, 112−113: 7−12.

[2] EI-ESKANDARANY M S, MAHDAY A A, AHMED H A , AMER A H. Synthesis and characterizations of ball-milled nanocrystalline WC and nanocomposite WC−Co powders and subsequent consolidations [J]. Journal of Alloys and Compounds, 2000, 312: 315−325.

[3] WU Chong-hu. Preparation of ultrafine tungsten powders by in-situ hydrogen reduction of nano-needle violet tungsten oxide [J]. International Journal of Refractory Metals and Hard Materials, 2011, 29: 686−691.

[4] SARIN V K. Morphological changes occurring during reduction of WO_3 [J]. Journal of Materials Science, 1975, 10: 593−598.

[5] SCHUBERT W D, LASSNER E. Production and characterization of hydrogen-reduced submicron tungsten powders. Part II: Controlled decomposition of APT and hydrogen reduction of the oxides [J]. International Journal of Refractory Metals and Hard Materials, 1991, 10: 171−183.

[6] SUN Ye-xi, SU Wei, YANG Hai-lin, RUAN Jian-ming. Effects of WC particle size on sintering behavior and mechanical properties of coarse grained WC−8Co cemented carbides fabricated by unmilled composite powders [J]. Ceramics International, 2015, 41: 14482−14491.

[7] ZHONG Yang, SHAW L L. Growth mechanisms of WC in WC−5.75wt.%Co [J]. Ceramics International, 2011, 37: 3591−3597.

[8] LONG Yan, GUO Wen-jing, LI Ying. Bimodal-grained Ti fabricated by high-energy ball milling and spark plasma sintering [J]. Transactions of Nonferrous Metals Society of China, 2016, 26: 1170−1175.

[9] BROOKES K J A. World directory and handbook of hard metals and hard materials: International carbide data [M]. 5th ed. East Barnet, United Kingdom: Metal Powder Industry, 1992: 37−41.

[10] ENAYATI M H, ARYANPOUR G R, EBNONNASIR A. Production of nanostructured WC−Co powder by ball milling [J]. International Journal of Refractory Metals and Hard Materials, 2009, 27: 159−163.

[11] METZGER M J, GLASSER D, HAUSBERGER B, HILDEBRANDT D, GLASSER B J. Use of the attainable region analysis to optimize particle breakage in a ball mill [J]. Chemical Engineering Science, 2009, 64: 3766−3777.

[12] RAIHANUZZAMAN R M, JEONG T S, GHOMASHCHI R, XIE Z H, HONG S J. Characterization of short-duration high-energy ball milled WC−Co powders and subsequent consolidations [J]. Journal of Alloys and Compounds, 2014, 615(S): s564−s568.

[13] HEWITT S A, KIBBLE K A. Effects of ball milling time on the synthesis and consolidation of nanostructured WC−Co composites [J]. International Journal of Refractory Metals and Hard Materials, 2009, 27: 937−948.

[14] CHEN Min, TANG Ai-tao, XIAO Xuan. Effect of milling time on carbothermic reduction of ilmenite [J]. Transactions of Nonferrous Metals Society of China, 2015, 25: 4201−4206.

[15] KURLOV A S, GUSEV A I. High-energy milling of nonstoichiometric carbides: Effect of nonstoichiometry on particle size of nanopowders [J]. Journal of Alloys and Compounds, 2014, 582: 108−118.

[16] LI Rui, QIN Ming-li, LIU Cheng-cheng, CHEN Zheng, WANG Xuan-li, QU Xuan-hui. Particle size distribution control and related properties improvements of tungsten powders by fluidized bed jet milling [J]. Advanced Powder Technology, 2017, 28: 1603−1610.

[17] LI Ping, SUN Da-zhi, WANG Xue, XUE Ke-min, HUA Rui, WU Yu-cheng. Microstructure and thermal stability of sintered pure tungsten processed by multiple direction compression [J]. Transactions of Nonferrous Metals Society of China, 2018, 28: 461−468.

[18] LECOQ O, CHOUTEAU N, MEBTOUL M, LARGE J F, GUIGON P. Fragmentation by high velocity impact on a target: A material grindability test [J]. Powder Technology, 2003, 133: 113−124.

[19] SHAIBANI M E, GHAMBARI M. Characterization and comparison of gray cast iron powder produced by target jet milling and high energy ball milling of machining scraps [J]. Powder Technology, 2011, 212: 278−283.

[20] PALANIANDY S, AZIZLI K A M, HUSSIN H, HASHIM S F S. Effect of operational parameters on the breakage mechanism of silica in a jet mill [J]. Minerals Engineering, 2008, 21: 380−388.

[21] WANG Yan-min, FORSSBERG E. Enhancement of energy efficiency for mechanical production of fine and ultra-fine particles

in comminution [J]. China Particuology, 2007, 5: 193−201.
[22] PALANIANDY S, AZIZLI K A M, HUSSIN H, HASHIM S F S. Mechanochemistry of silica on jet milling [J]. Journal of Material Processing Technology, 2008, 205: 119−127.
[23] MELNIKOVA I P, VOROZHEIKIN V G, USANOV D A. Correlation of emission capability and longevity of dispenser cathodes with characteristics of tungsten powders [J]. Applied Surface Science, 2003, 215: 59−64.
[24] PFEIFER J, BADALJAN E, TEKULA-BUXBAUM P, KOVA´CS T, GESZTI O, TO´TH A L, LUNK H J. Growth and morphology of $W_{18}O_{49}$ crystals produced by microwave decomposition of ammonium paratungstate [J]. Journal of Crystal Growth, 1996, 169: 727−733.
[25] SANTALA M K, GLAESER A M. Surface-energy-anisotropy-induced orientation effects on rayleigh instabilities in sapphire [J]. Surface Science, 2006, 600: 782−792.
[26] CHENG Peng, GAO Shu, LI Xu-sheng. Evaluation of a wide range laser particle size analysis and comparison with pipette and sieving methods [J]. Acta Sedimentologica Sinica, 2001, 19: 449−455. (in Chinese)
[27] KOZAWA K, SETO T, OTANI Y. Development of a spiral-flow jet mill with improved classification performance [J]. Advanced Powder Technology, 2012, 23: 601−606.
[28] WANG Yan-min, PENG Fei. Parameter effects on dry fine pulverization of alumina particles in a fluidized bed opposed jet mill [J]. Powder Technology, 2011, 214: 269−277.
[29] LU Xin, LIU Cheng-cheng, ZHU Lang-ping, QU Xuan-hui. Influence of process parameters on the characteristics of TiAl alloyed powders by fluidized bed jet milling [J]. Powder Technology, 2014, 254: 235−240.
[30] LI Rui, QIN Ming-li, HUANG Hua, LIU Cheng-cheng, CHEN Zheng, HUANG Min, ZHANG Lin, QU Xuan-hui. Fabrication of fine-grained spherical tungsten powder by radio frequency (RF) inductively coupled plasma spheroidization combined with jet milling [J]. Advanced Powder Technology, 2017, 28: 3158−3163.
[31] MACDONALD R, ROWE D, MARTIN E, GORRINGE L. The spiral jet mill cut size equation [J]. Powder Technology, 2016, 299: 26−40.
[32] SANTOS M A P D, COSTA C A. Comminution of silicon carbide powder in a planetary mill [J]. Powder Technology, 2006, 169: 84−88.
[33] ZAK A K, MAJID W H A, ABRISHAMI M E, YOUSEFI R. X-ray analysis of ZnO nanoparticles by Williamson-Hall and size-strain plot methods [J]. Solid State Sciences, 2011, 13: 251−256.
[34] GUO Zhi-xing, XIONG Ji, YANG Mei, XIONG Su-jian, CHEN Jian-zhong, WU Yue-mei, FAN Hong-yuan, SUN Lan, WANG Jun, WANG Hui. Dispersion of nano-TiN powder in aqueous media [J]. Journal of Alloys and Compounds, 2010, 493: 362−367.
[35] YIN Yan-fei, XU Wei, SUN Qiao-yan, XIAO Lin, SUN Jun. Deformation and fracture behavior of commercially pure titanium with gradient nano-to-micron-grained surface layer [J]. Transactions of Nonferrous Metals Society of China, 2015, 25: 738−747.
[36] CAO Jun, LI Fu-guo, MA Xin-kai, SUN Zhan-kun. Tensile stress−strain behavior of metallic alloys [J]. Transactions of Nonferrous Metals Society of China, 2017, 27: 2443−2453.
[37] SIWAK P, GARBIEC D. Microstructure and mechanical properties of WC−Co, WC−Co−Cr_3C_2 and WC−Co−TaC cermets fabricated by spark plasma sintering [J]. Transactions of Nonferrous Metals Society of China, 2016, 26: 2641−2646.
[38] CAO Rui-jun, LIN Chen-guang, JIA Cheng-chang. Measure the bonding strength of aggregates in ultrafine WC powder [J]. Cemented Carbide, 2009, 26: 1−6. (in Chinese)
[39] CHEN Jie, LIN Chen-guang, HU Xue-sheng. Strength of aggregates in ultrafine WC powder [J]. Powder Metallurgy Industry, 2008, 18: 25−29. (in Chinese)
[40] WARRAN R, WALDRON M B. Microstructural development during liquid phase sintering of cemented carbides [J]. Powder Metallurgy, 1972, 15: 166−201.
[41] GUO Sheng-da, BAO Rui, YANG Ping, LIU Liang, YI Jian-hong. Morphology and carbon content of WC−6%Co nanosized composite powders prepared using glucose as carbon source [J]. Transactions of Nonferrous Metals Society of China, 2018, 28: 722−728.
[42] SCHUBERT W D, BOCK A, LUX B. General aspects and limits of conventional ultrafine WC powder manufacture and hard metal production [J]. International Journal of Refractory Metals and Hard Materials, 1995, 13: 281−296.
[43] KANG M K, KIM D Y, HWANG N M. Ostwald ripening kinetics of angular grains dispersed in a liquid phase by two-dimensional nucleation and abnormal grain growth [J]. Journal of the European Ceramic Society, 2002, 22: 603−612.
[44] TAN Yin-guo, HUANG Li-shan. Dual grain structure cemented carbide [J]. Cemented Carbide, 1992(2): 10−14. (in Chinese)

气流粉碎对超细 WC 粉体微观应变行为及团粒破碎行为的影响

孙亚丽[1,2]，刘清才[1]，黄 新[1,3]，张发兴[3]，杨 剑[1]，梅 华[4]

1. 重庆大学 材料科学与工程学院，重庆 400044；2. 四川轻化工大学 材料科学与工程学院，自贡 643000；
3. 四川轻化工大学 化学工程学院，自贡 643000；4. 株洲钻石切削刀具股份有限公司，株洲 412007

摘 要：分别采用 Williamson−Hall 和单轴压缩法研究经气流粉碎和球磨处理后的超细 WC 粉体的微观应变及其应力−应变关系，并研究 WC 粉体中团粒破碎行为。以采用不同处理方法得到的 WC 粉体为原料制备 WC−10%Co 硬质合金，并对其性能进行分析。结果表明：相较于球磨处理得到 WC 粉体，经气流粉碎处理得到的 WC 粉体的微观应变显著降低；由于粉体中团粒的消除和晶格应变的减小，采用气流粉碎的 WC 粉体制备的硬质合金具备更加优良的综合性能，其抗弯强度达到 4260 MPa。

关键词：超细 WC 粉体；微观应变；应力−应变关系；气流粉碎；团粒破碎机理

(Edited by Wei-ping CHEN)